Tailoring the competition between electric dipole and magnetic dipole emission in Eu-doped cubic sesquioxide M_2O_3 ($M = \mathrm{Sc},\ \mathrm{Y},\ \mathrm{La}$)

Mu Lan,[1] Xiaofeng Wang,[2] Linxi Xie,[1] Dechao Meng,[2] Rong Wang,[3] Yu Song,[4] Song Sun,[2,*] and Su-Huai Wei[5,†,‡]

[1] *College of Optoelectronic Engineering, Chengdu University of Information Technology, Chengdu 610225, China*
[2] *Microsystem and Terahertz Research Center, China Academy of Engineering Physics, Chengdu 610200, China*
[3] *Institute of Advanced Semiconductors & Zhejiang Provincial Key Laboratory of Power Semiconductor Materials and Devices, Hangzhou Innovation Center, Zhejiang University, Hangzhou 311200, China*
[4] *College of Physics and Electronic Information Engineering, Neijiang Normal University, Yibin 641100, China*
[5] *Materials and Energy Division, Beijing Computational Science Research Center, Beijing 100193, China*

(Received 10 January 2024; revised 8 May 2024; accepted 1 July 2024; published 22 July 2024)

With an explosive increase in demand for efficient luminescent materials in integrated optical systems, research on lanthanide ion-doped cubic sesquioxide ceramics has become important and attractive. Because of the large doping capability of lanthanide atoms and a low preparation temperature that is much lower than the melting point, sesquioxides have demonstrated promising potential as a host matrix in solid-state laser gain media. Here, for the first time, we demonstrate that two types of cation sites with different symmetries in cubic sesquioxides could empower effective manipulation of the luminescence properties of lanthanide dopants, leading to either magnetic dipole (MD) or electrical dipole (ED) emission, respectively. Using rigorous first-principle calculations, the luminescence properties of Eu-doped sesquioxide M_2O_3 ($M = \mathrm{Sc},\ \mathrm{Y},\ \mathrm{La}$) are systematically investigated, unveiling the underlying competition mechanisms between MD and ED spontaneous emission. Through analyzing the formation energies of Eu dopants and intrinsic defects, the impact of strain and temperature on the doping concentration and dopant sites of Eu in sesquioxide is unambiguously elucidated, facilitating effective and selective manipulation of MD and ED emission.

DOI: 10.1103/PhysRevApplied.22.014054

I. INTRODUCTION

Sesquioxides represent a special group of metal oxides, for which the ratio between the number of metal atoms and oxygen atoms is 2:3. Among them, cubic sesquioxides M_2O_3 ($M = \mathrm{Sc},\ \mathrm{Y},\ \mathrm{La}$) are outstanding host materials for rare-earth lanthanide-based solid-state lasers. Their large bandgaps naturally lead to high transparency for the convenient excitation and radiation of lanthanide atoms, while their low phonon energies serve to inhibit nonradiative transition processes, potentially improving the laser signal-to-noise ratio and energy conversion efficiency, respectively. Furthermore, the high solubility of lanthanide elements in cubic sesquioxides enables strong laser emission intensity, while the high thermal conductivity allows for efficient heat extraction and dissipation during high-power laser operation. These unique advantages have triggered the widespread studies of lanthanide-doped sesquioxides as efficient luminescent materials and facilitated the development of high-power solid-state lasers for integrated optical systems [1–7]. At present, Eu-doped cubic sesquioxide Y_2O_3 has already been utilized as a commercial red-light source for several decades and is also widely used in cathode-ray tubes and plasma display devices [8–10]. Moreover, a substantial number of studies on other lanthanide-doped sesquioxide systems are actively being conducted to pursue higher luminescence efficiency, improved monochromaticity, and more stable operations [11–14].

Although it might seem that the luminescence properties of lanthanide-doped sesquioxides have already been comprehensively studied, the exotic magnetic dipole (MD) emission feature of lanthanide dopants brings radically new physical insights. For a long time, MD emission has been considered to be insignificant at optical frequencies due to its intrinsically much weaker emission strength compared with that of the electric dipole (ED) transition counterpart [15,16]. This perception has been challenged since the discovery of trivalent lanthanide ions

*Contact author: sunsong_mtrc@caep.cn
†Contact author: suhuaiwei@eitech.edu.cn
‡Present address: Eastern Institute of Technology, Ningbo 315200, China.

(i.e., Eu^{3+}, Er^{3+}, and so on), whose incompletely filled localized f-electron energy levels and heavy atom character allow for strong spin-orbital interactions, which exhibit a strong MD transition that is comparable to the ED transition [17–22]. In addition, the recent development in optical metamaterials and nanophotonics grants unrivaled capability to tailor local optical fields and enhance MD spontaneous emission by trivalent lanthanide ions, opening unlimited opportunities beyond convention applications involving only ED emission, such as optically induced magnetism, nanoscale magnetic probe, quantum memory and quantum sensing, among others [23–30]. Regardless, an efficient emitting material with properly controlled MD and ED features is the key premise and lays the cornerstone for both classical and emerging applications.

In the visible regime, Eu^{3+} is promising as an MD or ED emitter since it exhibits an intrinsic narrow linewidth MD transition at ∼592 nm, corresponding to the intra f–f electronic transitions of $5D^0 \rightarrow 7F^1$, as well as an intrinsic ED emission due to the $5D^0 \rightarrow 7F^2$ transition at a nearby wavelength ∼612 nm. Although pure MD and ED emission are highly desirable for certain applications, it is not easy to manipulate the Eu^{3+} transition properties via conventional approaches since the chemical environment has minimal influence on the localized. Nevertheless, it was found that the crystal field symmetry at the Eu^{3+} site could significantly modify the relative luminescence intensities of MD and ED emission, by altering the transition selection rules when embedded in a certain lattice matrix. The intensity of the $5D^0 \rightarrow 7F^1$ MD emission is strong only when Eu^{3+} occupies an inversion site, whereas the $5D^0 \rightarrow 7F^2$ ED transition dominates when Eu^{3+} occupies a noninversion site [19]. According to this principle, the existence of both inversion and noninversion doping sites in cubic sesquioxides would naturally lead to competition between the emission via an MD and an ED at Eu^{3+}. However, the luminescence properties of Eu-doped sesquioxides appear to vary among different experimental reports. For instance, Avram *et al.* have reported a strong MD emission at Eu in Y_2O_3 [31], while Kamal *et al.* have found a dominant ED emission peak in the same system [32]. To maximize the MD or ED emission in Eu-doped sesquioxides, it is essential to understand its underlying doping mechanism and, eventually, derive the optimized doping conditions where Eu^{3+} atoms could selectively occupy inversion or noninversion symmetry sites as much as possible [33].

In this work, the Eu^{3+} doping properties in M_2O_3 ($M = Sc,\ Y,\ La$) sesquioxides are systematically investigated and the competition mechanisms between the emission via an MD and an ED are clearly elucidated. Using rigorous first-principle calculations, the allowable range of chemical potential values for each element is obtained under thermodynamic equilibrium doping conditions, which shows that proper growth strategies of sesquioxides could be formulated to customize the Eu^{3+} doping proportions to empower selective improvement of MD or ED emission. It has been found that tensile strains and high growth temperatures are beneficial for ED emission from Eu-doped sesquioxides. On the other hand, compressive strains and low growth temperatures are preferred to achieve high-purity MD luminescence, while the suppression of metal vacancy and O interstitial is also needed.

II. METHODS

Spin-polarized first-principles calculations are conducted under the density functional theory (DFT) framework via the Vienna *ab initio* simulation package (VASP) [34] with the projector augmented wave pseudopotentials [35]. The exchange and correlation interaction between electrons is described using the strongly constrained and appropriately normed semilocal density functional (SCAN) meta-generalized gradient approximation (metaGGA) [36,37]. The hybrid functional theory of HSE06, including 25% nonlocal Hartree-Fock exchange, is manipulated to calculate electronic dispersions to correct the underestimated bandgaps [38]. Semicore electrons of Sc ($3s^2 3p^6 4s^2 3d^1$), Y ($4s^2 4p^6 5s^2 4d^1$), La ($5s^2 5p^6 6s^2 5d^1$), and Eu ($5s^2 5p^6 6s^2 4f^7$) are explicitly treated, while a $2s^2 2p^4$ configuration is used for O. A kinetic-energy cut-off of 520 eV is set, and electronic energy minimization is performed with a tolerance of 10^{-6} eV, while the force on each atom is converged within 0.02 eV/Å. All the calculations are carried out using a large $2 \times 2 \times 2$ supercell that contains 320 atoms for a pristine structure.

III. RESULTS AND DISCUSSIONS

Sesquioxides M_2O_3 ($M = Sc,\ Y,\ La$) exhibit bixbyite structures in the cubic crystal form, belonging to the space group $Ia\bar{3}$ with T_h^7 symmetry, where two different M sites are presented. The unit cell of M_2O_3 contains 24 O atoms and 16 M atoms; each M atom is bonded to 6 atoms to build MO_6 octahedra and each O atom is bonded to 4 M atoms, as shown in Fig. 1. The M atoms are distributed across two inequivalent sites: one-quarter of M atoms are located at S_6 sites, serving as the inversion center of MO_6 octahedra, while the other three-quarters of M atoms are found at C_2 sites, which lack inversion symmetries.

The calculated lattice constants of the sesquioxides Sc_2O_3, Y_2O_3, and La_2O_3 are 9.839 Å, 10.598 Å, and 11.315 Å, respectively, which are close to the experimental values of 9.85 Å, 10.60 Å, and 11.36 Å [39,40]. The bond lengths of the sesquioxides Sc_2O_3, Y_2O_3, and La_2O_3 are around the range 2.085–2.161 Å, 2.245–2.332 Å, and 2.389–2.510 Å, respectively. Since the elements Sc, Y, and La belong to the same IIIB group in the periodic table, the lattice constant and bond length of

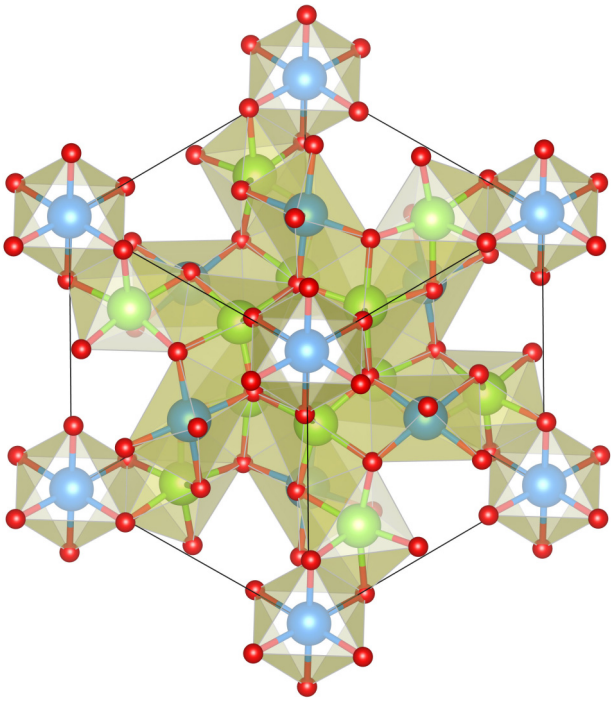

FIG. 1. Lattice structure of sesquioxide M_2O_3 ($M = $ Sc, Y, La). Red small balls stand for O atoms and blue and green large balls represent M atoms with S_6 and C_2 symmetry, respectively.

the corresponding sesquioxide gradually grow with the increase of the metal atomic radius. Despite the chemical similarity of Sc, Y, and La, their sesquioxides demonstrate distinct electronic structure characteristics. From the band structures depicted in Fig. 2(a), it is found that Sc_2O_3 is a direct bandgap semiconductor with valence band maximum (VBM) and conduction band minimum (CBM) located at the Brillouin zone center. Since the sesquioxide structure contains an inversion center and the electric dipole operator is of odd parity, strong optical transitions are only allowed between two states that exhibit opposing parities according to the selection rules. However, the VBM state at the Γ point is threefold degenerate with T_u symmetry, while the CBM state is nondegenerate with A_u symmetry. Thus, a zero optical transition matrix element at Γ point prevents direct VBM to CBM transition. Instead, the transition from VBM to a conduction band state, which is 0.58 eV above the CBM (T_g symmetry), is permissible. Similarly, the transition from a valence band state, which is 0.74 eV below the VBM (T_g symmetry), to CBM is feasible. As a result, Sc_2O_3 exhibits a larger optical gap than the electronic gap, which is similar to In_2O_3 [41]. For Y_2O_3 and La_2O_3, as shown in Figs. 2(b) and 2(c), respectively, both behave as indirect bandgap semiconductors with the CBM located at the Γ point. Their difference is that the VBM of Y_2O_3 is situated near the midpoint of the Γ–H high-symmetry line, whereas the VBM of La_2O_3 is located at the H point. Considering that the SCAN function may underestimate the bandgaps, we manipulated the HSE06 hybrid functional theory to obtain the bandgap of about 5.69 eV, 5.67 eV, and 4.96 eV for Sc_2O_3, Y_2O_3, and La_2O_3, respectively. The calculated large gaps are consistent with experimental values around the range of 5.7–6.2 eV, suggesting that the three sesquioxides are transparent wide-bandgap semiconductors [42–44], making them potentially ideal matrix materials for Eu^{3+} luminescence phosphors in the visible regime.

When Eu is doped into sesquioxides M_2O_3 ($M = $ Sc, Y, La), it can be either in the form of substitution or as an interstitial dopant. Because of the co-existence of two types of M sites, Eu can serve as two distinct substitutes: one functions as an inversion center on the S_6 site (referred to as Eu_{M1}), which may lead to dominant MD emission, while the other is located on the C_2 site (referred to as Eu_{M2}) without inversion symmetry, which may lead to dominant ED emission. As a result, the luminescent properties of Eu-doped sesquioxides M_2O_3 could be tailored by appropriately formulating the doping strategy. From Fig. 3(a), it is evident that the doped Eu atom can form bonds with six O atoms, regardless of whether it is located at the S_6 site or the C_2 site. In Figs. 3(b)–3(d), we compare the Eu-O and the intrinsic M-O bond lengths. When Eu substitutional doping is present in Sc_2O_3 and Y_2O_3, it could form bonds with neighboring O atoms that are longer than intrinsic M-O bond lengths. Conversely, when Eu is doped into La_2O_3, the Eu-O bond lengths are shorter compared with the La-O bonds. This is due to the fact that the Eu atom possesses a larger radius (0.947 Å) than Sc (0.745 Å) and Y (0.9 Å), yet a smaller one compared with La (1.032 Å). It could also be noticed that the Eu_{M1}-O bonds are the same length, while Eu_{M2}-O bonds could be categorized into three distinct pairs with different lengths.

To clarify the doping properties, the formation energies of doped Eu can be evaluated as a function of atomic chemical potentials and the electron Fermi levels, i.e.,

$$\Delta H_f(\alpha, q) = \Delta E(\alpha, q) + n_O\mu_O + n_M\mu_M + n_{Eu}\mu_{Eu} + qE_F, \quad (1)$$

where

$$\Delta E(\alpha, q) = E(\alpha, q) - E(M_2O_3) + n_O E(O) + n_M E(M) + n_{Eu}E(Eu) + qE_{VBM},$$

where E_F is the Fermi level referenced to the VBM of M_2O_3. Moreover, μ_O, μ_M, and μ_{Eu} are the chemical potentials of O, M, and Eu in terms of their elemental solids with energies of $E(O)$, $E(M)$, and $E(Eu)$, respectively. The variable n represents the number of atoms transferred from

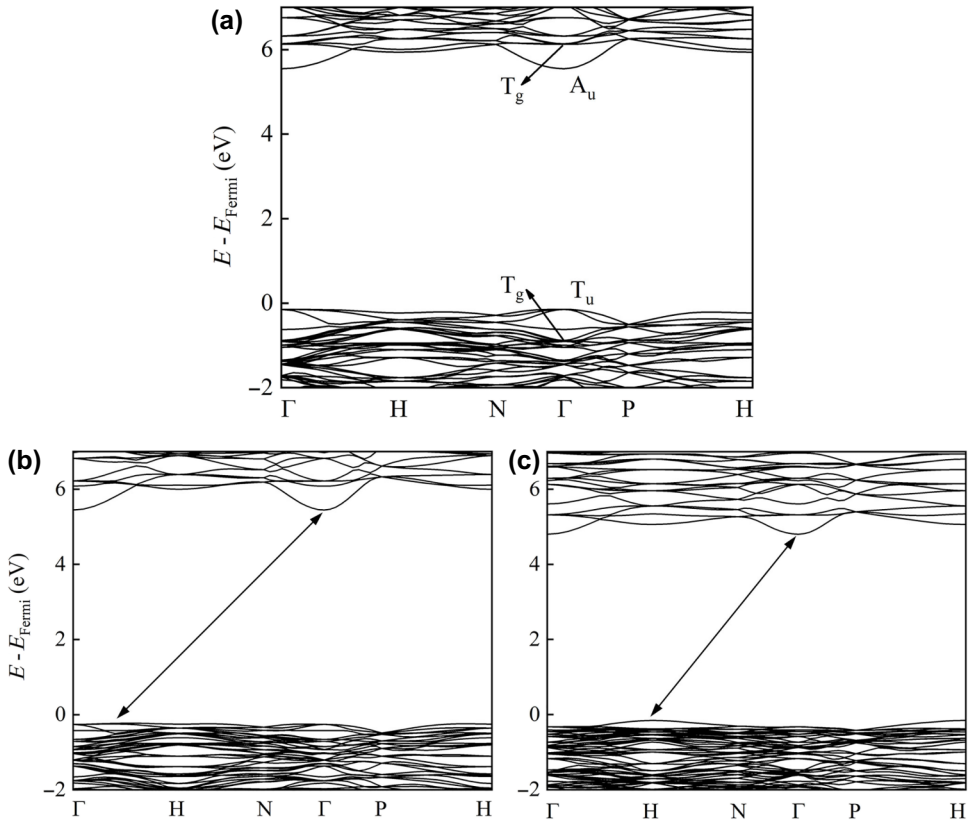

FIG. 2. Band structures of (a) Sc_2O_3, (b) Y_2O_3, and (c) La_2O_3.

the supercell to the reservoirs in the creation of defect cells, while q denotes the charge state of the defect α. Furthermore, a correction is incorporated to account for the alignment of the averaged electrostatic potentials by the core level line-up.

According to Eq. (1), the formation energies of doped Eu are influenced by the elemental chemical potentials, which are sensitive to growth conditions. Under thermal equilibrium growth conditions, the permissible values of each element's chemical potential μ are restricted. To avoid the precipitation of elemental substances, the chemical potentials are limited by

$$\mu_{\mathrm{Eu}} \leq 0, \quad \mu_{\mathrm{O}} \leq 0, \quad \mu_M \leq 0, \quad M = (\mathrm{Sc},\ \mathrm{Y},\ \mathrm{La}), \tag{2}$$

where $\mu = 0$ is defined as the energy of the most stable solid or gas phase of each element. Then, in order to preserve the stable phase of compounds, the combined chemical potentials of their constituent elements must be equal to the formation energies of sesquioxides, i.e.,

$$2\mu_M + 3\mu_{\mathrm{O}} = \Delta H_f\,(M_2\mathrm{O}_3), \quad M = (\mathrm{Sc}, \mathrm{Y}, \mathrm{La}). \tag{3}$$

To prevent the precipitation of secondary phases of Eu oxides, these chemical potentials are further limited by

$$m\mu_{\mathrm{Eu}} + n\mu_{\mathrm{O}} \leq \Delta H_f\,(\mathrm{Eu}_m\mathrm{O}_n). \tag{4}$$

Here, we take into account the stable phases of metal oxides. The calculated formation energies of the compounds are compared with experimental values in Table I, which are in good agreement.

In Fig. 4(a), we have compared the formation energies of Eu point defects in Sc_2O_3 under O-poor and O-rich growth conditions. It is found that the Eu interstitials could be easily formed in p-type Sc_2O_3 since the formation energies of Eu substitutes are relatively high. This infers that an O-poor condition is not suitable for Eu doping in M sites. In contrast, the formation energies of Eu interstitials are too high to be important under O-rich conditions, and the Eu substitute doping becomes much more favorable. The formation energies of Eu isovalent doping are about 0.57 eV on the S_6 site and 0.63 eV on the C_2 site. Despite the lower formation energy of Eu_{M1} on isovalent doping, Eu_{M2} could be dominant when the Fermi level is close to VBM or CBM, where Eu_{M2} exhibits lower formation energy. This corresponds to the deep $\langle +3|+2\rangle$, $\langle +2|+1\rangle$, and $\langle +1|0\rangle$ donor transition levels at about $E_F = 0.03$, 0.04,

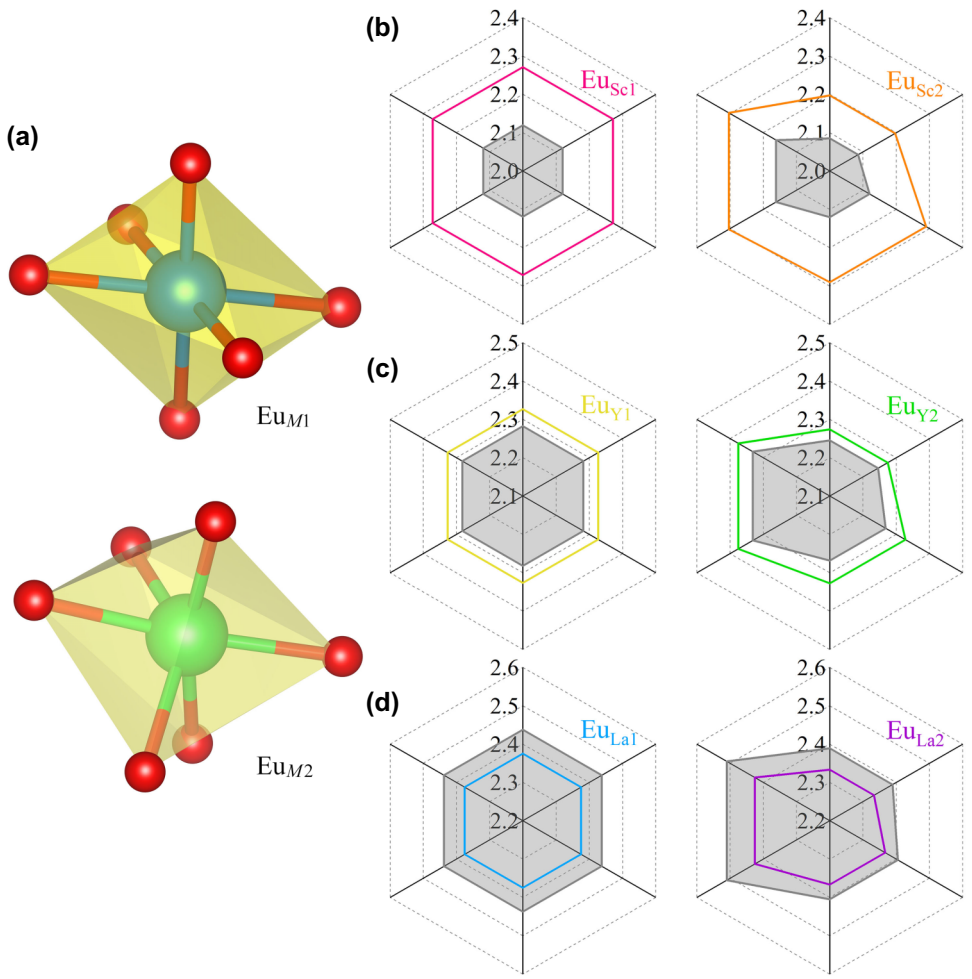

FIG. 3. (a) Geometrical structure of Eu_{M1} at the S_6 site and Eu_{M2} at the C_2 site. (b) Comparison between Eu-O and Sc-O bond lengths in Sc_2O_3 with Eu on the S_6 site and C_2 site, respectively. (c) Comparison between Eu-O and Y-O bond lengths in Y_2O_3. (d) Comparison between Eu-O and La-O bond lengths in La_2O_3. Grayscales on the axis correspond to the intrinsic M-O bond lengths in sesquioxides, while the colored scales correspond to the Eu-O bond lengths.

and 0.38 eV, respectively, and deep $\langle 0|-1\rangle$ acceptor transition level at about $E_F = 2.78$ eV for Eu_{M2}. Furthermore, Eu_{M1} has deep $\langle +2|+1\rangle$ and $\langle +1|0\rangle$ donor transition levels at about $E_F = 0.06$ and 0.18 eV, respectively. and a deep $\langle 0|-1\rangle$ acceptor transition level at about $E_F = 2.75$ eV. Considering the advantages of the exclusion of Eu interstitials and the effective doping of Eu substitutes, an O-rich growth condition is assumed hereafter.

TABLE I. Calculated and experimental formation energies of metal oxides. Experimental formation energies are from the Scientific Group Thermodata Europe (SGTE) Solid SUBstance database [45].

Compound	Calculated ΔH_f (eV/atom)	Experimental ΔH_f (eV/atom)
Sc_2O_3	−4.003	−3.956
Y_2O_3	−4.048	−3.949
La_2O_3	−3.848	−3.722
EuO (Fm-3m)	−3.156	−3.057
Eu_2O_3 (P-3m1)	−3.125	−3.437

In Eu-doped Y_2O_3 and La_2O_3, the situations are similar to those in Sc_2O_3 under O-rich conditions, as depicted in Figs. 4(b) and 4(c). As the ionic radius increases from Sc (0.745 Å) to Y (0.9 Å) and La (1.032 Å), the formation energies of the Eu substitution slightly decrease, which means that the Eu doping into these two sesquioxides is relatively easy. Although the formation energies of interstitials decrease compared with the Sc_2O_3 case, they are still much higher than that of Eu substitutions. Therefore, it can be concluded that the Eu interstitial barely exists under O-rich conditions for all three sesquioxides.

As the formation energies of Eu_{M1} and Eu_{M2} are very close, substitutions cannot be ignored. According to the aforementioned luminescence mechanism, Eu_{M1} substitution on the S_6 site mainly exhibits MD emission,

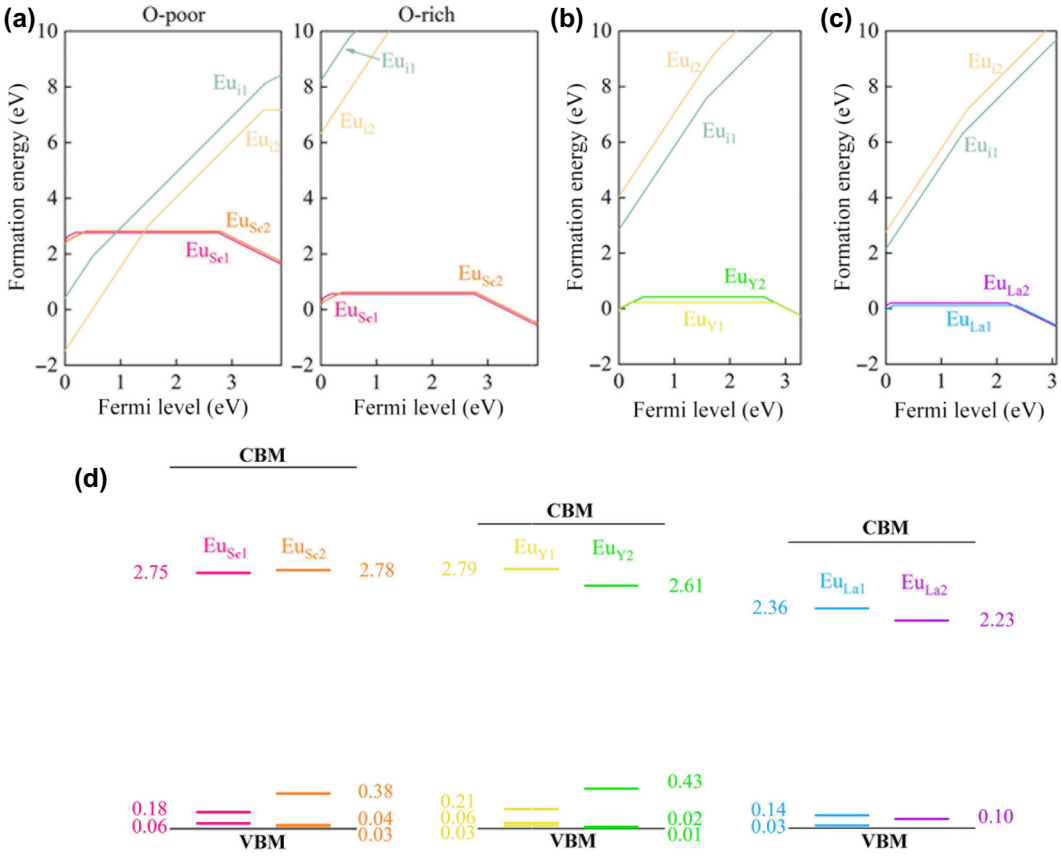

FIG. 4. Formation energies of Eu doping into (a) sesquioxide Sc_2O_3 under O-poor and O-rich conditions, (b) Y_2O_3 under O-rich conditions, and (c) La_2O_3 under O-rich conditions. (d) Charge transition levels of substitute Eu in sesquioxides Sc_2O_3, Y_2O_3, and La_2O_3.

while Eu_{M2} substitution on the C_2 site displays ED emission. Thus, tailoring the doping properties of Eu could lead to competition between the emission via an MD and an ED. The external strain has been proven to be an effective method to manipulate the doping properties in many semiconductors [46]. To simulate the hydrostatic strain on the sesquioxide lattice, we change the lattice constants along three dimensions equally and analyze the strain-induced changes in the formation energies of Eu_{M1} and Eu_{M2}. The results are illustrated in Fig. 5, where the formation energies of unstrained Eu_{M1} and Eu_{M2} are set as the references. Similar to dopant formation energies in most conventional semiconductors [47], the formation energies of Eu-doped sesquioxides exhibit nearly linear relationships with strain. We noticed that when Eu is doped into Sc_2O_3 and Y_2O_3, the tensile strain could make Eu substitutions energetically more favorable. Moreover, for Eu doping into La_2O_3, the introduction of compressive strain could increase the energetic favorability of Eu substitutions. This is also because the radius of Eu is larger than

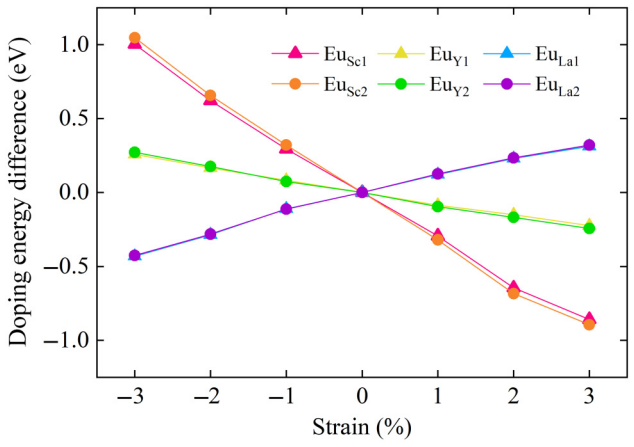

FIG. 5. Formation energy difference versus hydrostatic strain for Eu substitutions in sesquioxides.

TABLE II. Density of states effective masses of electrons and holes in sesquioxides.

Unit: electron inertia mass m_0	Sc_2O_3	Y_2O_3	La_2O_3
m_n^*	1.158	0.736	2.244
m_p^*	8.859	9.889	8.304

that of Sc and Y and smaller than that of La. In Eu-doped Sc_2O_3, the formation energies of Eu_{Sc1} and Eu_{Sc2} decrease with tensile strain but increase with compressive strain. In comparison, Eu_{Sc2} is more sensitive to strain changes, making it more energetically favorable with tensile strain and less energetically favorable with compressive strain. As a result, the application of compressive strain could increase the MD emission, while a tensile strain could enhance the ED emission of Eu in Sc_2O_3. These findings are in line with the experimental results in Ref. [15], which shows that $(Sc_{0.99}Eu_{0.01})_2O_3$ with a unit cell lattice constant of 9.849 Å displays a much stronger MD illumination under x-ray excitation compared with $(Sc_{0.92}Eu_{0.08})_2O_3$ with a larger unit cell lattice constant of 9.877 Å. In contrast, the formation energy differences between Eu_{M1} and Eu_{M2} in Y_2O_3 and La_2O_3 appear small with a strain ranging from −3% to 3%, so simply applying strain might not be a good approach when tuning their MD and ED emission.

Besides the hydrostatic strain, other strategies could influence the Eu doping properties in sesquioxides. According to our previous reports [33], growth temperature and doping concentration might have an impact on doping properties. In order to uncover the connection between doping properties and physical conditions (i.e., growth temperature and doping concentration), detailed balance equations are adopted to quantitatively describe the Eu doping mechanism in sesquioxides under O-rich conditions. We account for defects due to substitutions of Eu_{M1} and Eu_{M2} with different charge states, while interstitials with higher formation energies (see Fig. 3) are ignored for simplicity. Under equilibrium doping conditions, their densities follow the Boltzmann distributions, which are governed by

$$n(\mathrm{Eu}^i_{M1}) = N_{\mathrm{Eu}} \frac{g_i e^{-\Delta H_f(\mathrm{Eu}^i_{M1})/k_BT}}{\sum_{i=-1,0,1,2,3} g_i e^{-\Delta H_f(\mathrm{Eu}^i_{M1})/k_BT} + \sum_{i=-1,0,1,2,3} 3 \times g_i e^{-\Delta H_f(\mathrm{Eu}^i_{M2})/k_BT}}, \tag{5a}$$

$$n(\mathrm{Eu}^i_{M2}) = N_{\mathrm{Eu}} \frac{3g_i e^{-\Delta H_f(\mathrm{Eu}^i_{M2})/k_BT}}{\sum_{i=-1,0,1,2,3} g_i e^{-\Delta H_f(\mathrm{Eu}^i_{M1})/k_BT} + \sum_{i=-1,0,1,2,3} 3g_i e^{-\Delta H_f(\mathrm{Eu}^i_{M2})/k_BT}}, \tag{5b}$$

where N_{Eu} is the total doping concentration of Eu in sesquioxides and g_i are the degeneracy factors relating to possible electron occupations; these are 2, 1, 6, 15, and 20 for $Eu_M{}^{-1}$, $Eu_M{}^0$, $Eu_M{}^{+1}$, $Eu_M{}^{+2}$, and $Eu_M{}^{+3}$, respectively. The hole density p_0 in the valence band and electron density n_0 in the conduction band are functions of the Fermi level at a given temperature, which are given by

$$n_0 = N_c e^{-(E_c - E_F/k_BT)}, \quad N_c = 2\frac{(2\pi m_n^* k_B T)^{3/2}}{h^3}, \tag{6a}$$

$$p_0 = N_v e^{-(E_F - E_v/k_BT)}, \quad N_v = 2\frac{(2\pi m_p^* k_B T)^{3/2}}{h^3}, \tag{6b}$$

where Nc and Nv are the effective density of states of the conduction bands that can accept electrons and the valence bands that can accept holes, respectively. Moreover, $m_n{}^*$ and $m_p{}^*$ are the effective masses of electrons and holes in sesquioxides, respectively, which are derived by fitting the parabolic relationship of density of states near CBM and VBM, as introduced by Neufeld *et al.* (see Table II) [48].

Furthermore, the charge neutrality condition requires that

$$p_0 + \sum_{i=1,2,3} in(\mathrm{Eu}^i_{M1}) + \sum_{i=1,2,3} i' n(\mathrm{Eu}^{i'}_{M2}) = n_0 + n(\mathrm{Eu}^{-1}_{M1}) + n(\mathrm{Eu}^{-1}_{M2}). \tag{7}$$

Solving Eqs. (5)–(7), we can obtain the Fermi level and the proportion of Eu substitutions as a function of the growth temperature and doping concentration. First, the effect of temperature on the doping properties should be interrogated. From Eq. (5), we can evaluate the ratio between $Eu_{Sc1}{}^0$ and $Eu_{Sc2}{}^0$ as approximately

$$\frac{1}{3}\exp\frac{\Delta H_f(\mathrm{Eu}^0_{Sc2}) - \Delta H_f(\mathrm{Eu}^0_{Sc1})}{k_BT}.$$

Assuming that the defect formation energies are irrelevant with respect to temperature, $\Delta H_f(\mathrm{Eu}^0_{Sc2}) - \Delta H_f(\mathrm{Eu}^0_{Sc1})$ should be a positive constant. A high temperature could lead to a $Eu_{Sc1}{}^0$:$Eu_{Sc2}{}^0$ ratio close to 1/3, namely, the S_6:C_2 site ratio. In contrast, $Eu_{Sc1}{}^0$ could be dominant at room temperature. Thus, despite a large proportion of

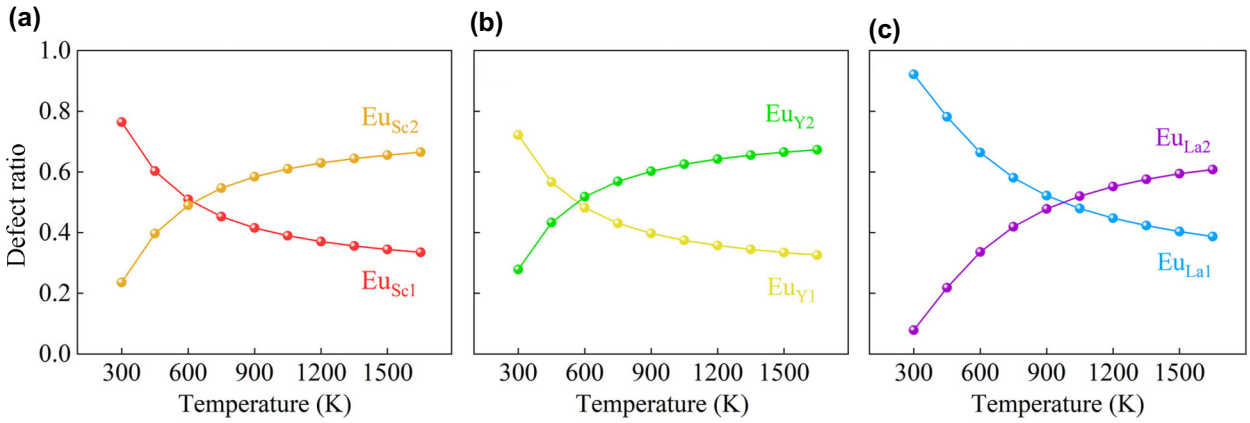

FIG. 6. Defect proportions of neutral Eu substitutions in Sc_2O_3, Y_2O_3, and La_2O_3 as functions of temperature.

$Eu_{Sc1}{}^0$ (present in over three quarters of the sites) at room temperature, $Eu_{Sc2}{}^0$ gains an advantage as the temperature increases above 750 K, which reaches a two-thirds occupation of sites at a temperature of 1650 K, as shown in Fig. 6. Similar conclusions can be obtained for Eu-doped Y_2O_3 and La_2O_3. The $Eu_{Y1}{}^0$:$Eu_{Y2}{}^0$ ratio changes from 72.1%:27.9% at room temperature to 32.6%:67.3% at a temperature of 1650 K, and the $Eu_{La1}{}^0$:$Eu_{La2}{}^0$ ratio changes from 92.1%:7.9% at room temperature to 38.7%:60.8% at a temperature of 1650 K. In short, controlling the temperature provides a powerful tool to manipulate the competition between the emission via MD or ED, whereby a lower and higher growth temperature leads to a favorable Eu^{3+} doping of the S_6 and C_2 sites and enhanced MD and ED emission, respectively.

Next, the influence of doping concentration on the doping properties of Eu needs to be investigated. Figure 7 illustrates the Fermi level, as well as the defect ratio of Eu substitutions in Sc_2O_3 under equilibrium growth conditions at a room temperature of 300 K. When the Eu doping concentration is low, the Fermi level monotonically decreases until it is pinned at about 1.57 eV above the VBM for a value higher than $10^{16}/cm^3$. When the Fermi level is close to the center of the bandgap, the dominant substitutions are $Eu_{Sc1}{}^0$ and $Eu_{Sc2}{}^0$. It is found that the Eu doping concentration can barely change the proportions of $Eu_{Sc1}{}^0$ (76.4%) and $Eu_{Sc2}{}^0$ (23.6%), which is also valid for Y_2O_3 and La_2O_3. The defect proportions of $Eu_{Y1}{}^0$ and $Eu_{Y2}{}^0$ are 72.1% and 27.9%, receptively, with the Fermi level pinned at about 1.52 eV for heavily Eu-doped Y_2O_3. In addition, the defect proportions of $Eu_{La1}{}^0$ and $Eu_{La2}{}^0$ are 92.1% and 7.9%, respectively, with the Fermi level pinned at about 1.23 eV for heavily Eu-doped La_2O_3. Thus, tuning the Eu doping concentration alone has a limited effect when manipulating the competition between emission via MD and ED.

Based on the emission mechanism, we can estimate the emission energy of Eu in the sesquioxides. The Eu^{3+} ^7F state has six spin-up f electrons in its electronic configuration, while the ^5D state, which can be reached with one spin-flip excitation, has five spin-up and one spin-down f electrons. Although the ground-state DFT

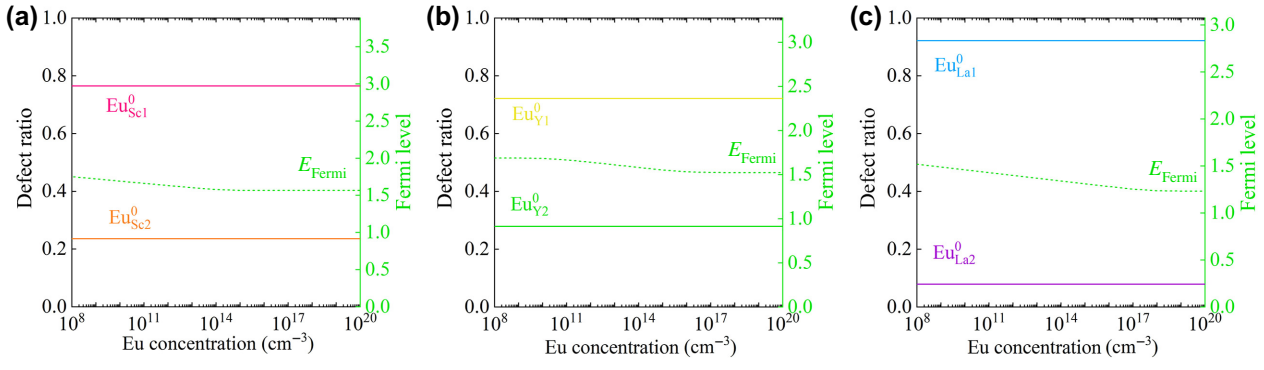

FIG. 7. Defect ratio of neutral substitutions and Fermi level as a function of total Eu doping concentration under thermodynamic equilibrium growth condition in Eu-doped (a) Sc_2O_3, (b) Y_2O_3, and (c) La_2O_3 at 300 K.

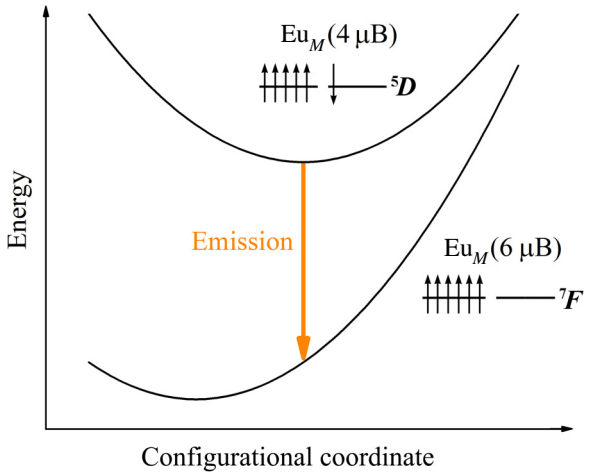

FIG. 8. Schematic of a configurational coordinate diagram.

calculation cannot typically handle the excited state, the energy difference between the $^7F_0$ and $^5D_0$ states can be accurately calculated as the energy difference of the high spin state of $^7F_0$ with 6 μ_B and the low spin state of $^5D_0$ with 4 μ_B, because of the localized nature of these states and error cancellation. The $^5D_0 \rightarrow {}^7F_0$ emission energies of Eu_{M1}, $\Delta E(Eu_{M1}^{em}) = E[Eu_{M1}(4\ \mu_B)] - E[Eu_{M1}(6\ \mu_B)]$, are schematically illustrated in the configurational coordinate diagram in Fig. 8, which are calculated as 2.163 eV, 2.809 eV, and 2.224 eV in Sc_2O_3, Y_2O_3, and La_2O_3, respectively, and are close to the experimental value of 2.138 eV (580 nm) [17].

Previous discussions have not considered the effect of intrinsic defects in Eu-doped sesquioxides. Actually, when the O element is abundant during sesquioxide growth, the introduction of M vacancy (V_M) and O interstitial (O_i) is highly probable. The existence of intrinsic defects could compensate the substitute dopants Eu_M, and even dominate the doping properties of Eu in sesquioxides. Figure 9 shows the formation energies of intrinsic defects, including substitutes and interstitials in sesquioxides under O-rich conditions. It is evident that the O interstitials have relatively low formation energies, which could compensate for the Eu substitutions at lower Fermi levels than previously estimated. A high O interstitial and M (M = Sc, Y, La) vacancy concentrations, which have been confirmed by Ref. [49], might potentially disrupt the inversion symmetry of Eu_{M1} sites, leading to a suppression of MD emission.

IV. CONCLUSION

In conclusion, our systematic investigation of Eu doping properties in cubic M_2O_3 (M = Sc, Y, La) sesquioxides has provided valuable insights into the competition mechanism between emission via an MD and an ED. Via rigorous first-principle calculations, the allowable range of chemical potential values for each element is determined under thermodynamic equilibrium doping conditions, allowing for properly formulating growth strategies to customize Eu doping proportions involving MD or ED emission. Our results suggest that tensile strains and high growth temperatures are beneficial for the ED emission from Eu-doped sesquioxides, while opposite growth conditions and suppression of metal vacancy and O interstitial are required for high-purity MD luminescence. These findings could provide important guidance for the development and optimization of high-performance Eu-doped sesquioxides for efficient luminescent applications. Furthermore, through the refinement of synthesis and growth conditions, there is potential to accurately regulate the doping ratios of other lanthanide-doped materials. This could pave the way

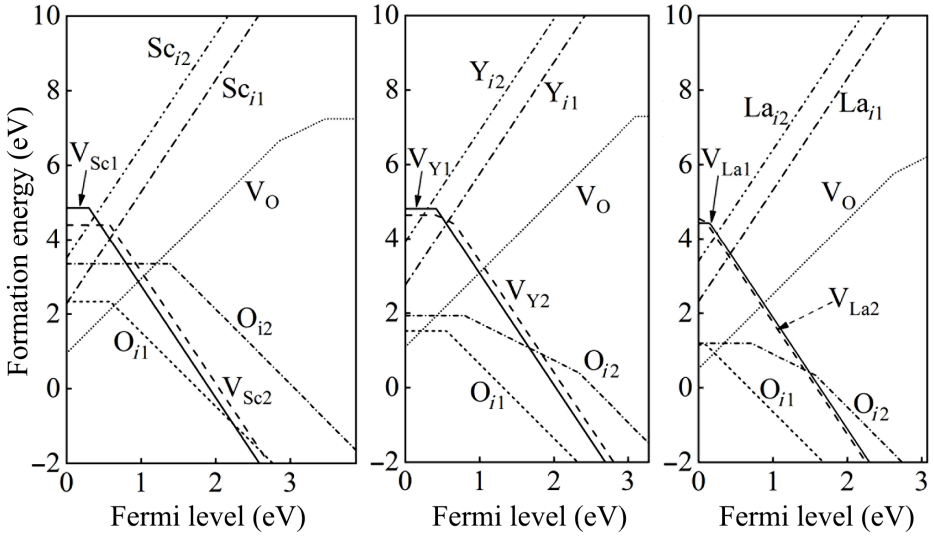

FIG. 9. Formation energies of intrinsic defects in sesquioxides under O-rich conditions.

for new avenues that enhance the emission properties of specific site-selective applications.

ACKNOWLEDGMENTS

This work was supported by the Scientific Research Foundation of CUIT (Grant No. KYTZ202172), the National Natural Science Foundation of China (Grants No. 62005256, No. 12088101, No. 11991060, and No. U2230402), the CAEP Innovation and Development Fund (Grant No. CX20200011), the Sichuan Science and Technology Program (Grant No. 2022ZYD0033), and the Natural Science Foundation of Sichuan Province (Grant No. 2022NSFSC0339).

[1] Q. Li, Y. Wang, J. Wang, J. Ma, M. Ni, H. Lin, J. Zhang, P. Liu, X. Xu, and D. Tang, High transparency Pr:Y_2O_3 ceramics: A promising gain medium for red emission solid-state lasers, J. Adv. Ceram. **11**, 874 (2022).

[2] G. Stanciu, L. Gheorghe, F. Voicu, S. Hau, C. Gheorghe, G. Croitoru, M. Enculescu, and R. P. Yavetskiy, Highly transparent Yb:Y_2O_3 ceramics obtained by solid-state reaction and combined sintering procedures, Ceram. Int. **45**, 3217 (2019).

[3] W. Liu, J. Li, B. Jiang, D. Zhang, and Y. Pan, Effect of La_2O_3 on microstructures and laser properties of Nd:YAG ceramics, J. Alloys Compd. **512**, 1 (2012).

[4] A. A. Yadav, A. C. Lokhande, J. H. Kim, and C. D. Lokhande, Supercapacitive activities of porous La_2O_3 symmetric flexible solid-state device by hydrothermal method, Int. J. Hydrogen Energy **41**, 18311 (2016).

[5] C. Gheorghe, A. Lupei, V. Lupei, A. Ikesue, and M. Enculescu, Intensity parameters of Tm^{3+} doped Sc_2O_3 transparent ceramic laser material, Opt. Mater. **33**, 501 (2011).

[6] P. G. Schunemann, M. S. Bowers, M. Dubinskiy, Y. Kaneda, C. J. Saraceno, and P. Camy, Advanced solid-state lasers: Feature issue introduction, Opt. Express **31**, 25718 (2023).

[7] A. Uvarova, P. Loiko, S. Kalusniak, E. Dunina, L. Fomicheva, A. Kornienko, S. Balabanov, A. Braud, P. Camy, and C. Kränkel, Stimulated-emission cross-sections of trivalent erbium ions in the cubic sesquioxides Y_2O_3, Lu_2O_3, and Sc_2O_3, Opt. Mater. Express **13**, 1385 (2023).

[8] R. B. Hunt, Jr and R. G. Pappalardo, Fast excited-state relaxation of Eu-Eu pairs in commercial Y_2O_3:Eu^{3+} phosphors, J. Lumin. **34**, 133 (1985).

[9] M. Buijs, A. Meyerink, and G. Blasse, Energy transfer between Eu^{3+} ions in a lattice with two different crystallographic sites: Y_2O_3:Eu^{3+}, Gd_2O_3:Eu^{3+}andEu_2O_3, J. Lumin. **37**, 9 (1987).

[10] G. Wakefield, E. Holland, P. J. Dobson, and J. L. Hutchison, Luminescence properties of nanocrystalline Y_2O_3:Eu, Adv. Mater. **13**, 1557 (2001).

[11] Y. Pan, X. Xie, Q. Huang, C. Gao, Y. Wang, L. Wang, B. Yang, H. Su, L. Huang, and W. Huang, Inherently Eu^{2+}/Eu^{3+} codoped Sc_2O_3 nanoparticles as high-performance nanothermometers, Adv. Mater. **30**, 1705256 (2018).

[12] D. S. Pytalev, D. Caurant, O. Majérus, H. Trégouët, T. Charpentier, and B. N. Mavrin, Structure and crystallization behavior of $La_2O_3 \cdot 3B_2O_3$ metaborate glasses doped with Nd^{3+} or Eu^{3+} ions, J. Alloys Compd. **641**, 43 (2015).

[13] G. Zhang, I. Milisavljevic, E. Zych, and Y. Wu, High-entropy sesquioxide X_2O_3 upconversion transparent ceramics, Scr. Mater. **186**, 19 (2020).

[14] L. Zheng, H. Wu, L. Zhang, Y. Luo, G.-H. Pan, X.-J. Wang, Z. Hao, and J. Zhang, Determination of cross-relaxation efficiency based on spectroscopy in thulium-doped rare-earth sesquioxides, Ceram. Int. **49**, 11060 (2023).

[15] L. Zhuang, H. Feng, S. Huang, Z. Zhang, W. Yong, R. Mao, and J. Zhao, The luminescent properties comparison of RE_2O_3:Eu (RE = Lu, Y, Sc) with high and low Eu doping concentrations, J. Alloys Compd. **781**, 302 (2019).

[16] L. D. Landau and E. Lifshitz, *Electrodynamics of Continuous Media* (Pergamon Press, Oxford, New York, Beijing, Frankfurt, 1984).

[17] M. Kasperczyk, S. Person, D. Ananias, L. D. Carlos, and L. Novotny, Excitation of magnetic dipole transitions at optical frequencies, Phys. Rev. Lett. **114**, 163903 (2015).

[18] Z. Q. Bian, K. Z. Wang, and L. P. Jin, Syntheses, spectroscopic and crystal structural studies of novel imidazo[4,5-f]1,10-phenanthroline derivatives and their Eu(III) ternary complexes with dibenzoylmethane, Polyhedron **21**, 313 (2002).

[19] Z. L. Fu, H. K. Yang, B. K. Moon, B. C. Choi, and J. H. Jeong, $La_2Sn_2O_7$:Eu^{3+} micronanospheres: Hydrothermal synthesis and luminescent properties, Cryst. Growth Des. **9**, 616 (2009).

[20] A. K. Kunti, N. Patra, R. A. Harris, S. K. Sharma, D. Bhattacharyya, S. N. Jha, and H. C. Swart, Local structure and spectroscopic properties of Eu^{3+}-Doped $BaZrO_3$, Inorg. Chem. **58**, 3073 (2019).

[21] S. M. Rafiaei, Effect of flux compounds on the luminescence properties of Eu^{3+} doped YBO_3 phosphors, Mater. Sci.-Poland **34**, 780 (2016).

[22] Y. Li, X. P. Gao, G. R. Li, G. L. Pan, T. Y. Yan, and H. Y. Zhu, Titanate nanofiber reactivity: Fabrication of $MTiO_3$ (M = Ca, Sr, and Ba) perovskite oxides, J. Phys. Chem. C **113**, 4386 (2009).

[23] S. Sun, D. Li, D. C. Wang, Z. Feng, W. Tan, and L. Wu, Empowering magnetic strong coupling and its application for nonlinear refractive index sensing, Nano Res. **15**, 7604 (2022).

[24] A. D. Utyushev, R. Gaponenko, S. Sun, A. Shcherbakov, A. Moroz, and I. L. Rasskazov, Generation of nearly pure and highly directional magnetic light in fluorescence of rare-earth ions, Phys. Rev. B **109**, 045413 (2024).

[25] S. Sun, W. Tan, and S.-H. Wei, *Emergent Micro- and Nanomaterials for Optical, Infrared, and Terahertz Applications* (CRC Press, Boca Raton, 2023).

[26] T. H. Taminiau, S. Karaveli, N. F. van Hulst, and R. Zia, Quantifying the magnetic nature of light emission, Nat. Commun. **3**, 979 (2012).

[27] V. V. Klimov, Spontaneous emission of an excited atom placed near a "left-handed" sphere, Opt. Commun. **211**, 183 (2002).

[28] V. V. Klimov and M. Ducloy, Allowed and forbidden transitions in an atom placed near an ideally conducting cylinder, Phys. Rev. A **62**, 043818 (2000).
[29] B. Rolly, B. Bebey, S. Bidault, B. Stout, and N. Bonod, Promoting magnetic dipolar transition in trivalent lanthanide ions with lossless Mie resonances, Phys. Rev. B **85**, 245432 (2012).
[30] M. K. Schmidt, R. Esteban, J. J. Sáenz, I. Suárez-Lacalle, S. Mackowski, and J. Aizpurua, Dielectric antennas - a suitable platform for controlling magnetic dipolar emission, Opt. Express **20**, 13636 (2012).
[31] D. Avram, B. Cojocaru, M. Florea, and C. Tiseanu, Advances in luminescence of lanthanide doped Y_2O_3: Case of S_6 sites, Opt. Mater. Express **6**, 1635 (2016).
[32] S. Nigam, C. S. Kamal, K. R. Rao, V. Sudarsan, and R. K. Vatsa, Eu^{3+} ions imminence impact on its photoluminescence in Y_2O_3 host, J. Lumin. **178**, 219 (2016).
[33] M. Lan, R. Wang, Z. H. Yang, X. F. Wang, S. Sun, and S.-H. Wei, Enhancing magnetic dipole emission in Eu-doped $SrMO_3$ (M = Ti, Zr, Hf): First-principles calculations, Phys. Rev. B **103**, 245201 (2021).
[34] G. Kresse and J. Furthmüller, Efficient iterative schemes for ab initio total-energy calculations using a plane-wave basis set, Phys. Rev. B **54**, 11169 (1996).
[35] P. E. Blöchl, Projector augmented-wave method, Phys. Rev. B **50**, 17953 (1994).
[36] J. Sun, A. Ruzsinszky, and J. P. Perdew, Strongly constrained and appropriately normed semilocal density functional, Phys. Rev. Lett. **115**, 036402 (2015).
[37] J. Sun, R. C. Remsing, Y. Zhang, Z. Sun, A. Ruzsinszky, H. Peng, Z. Yang, A. Paul, U. Waghmare, X. Wu, M. L. Klein, and J. P. Perdew, Accurate first-principles structures and energies of diversely bonded systems from an efficient density functional, Nat. Chem. **8**, 831 (2016).
[38] J. Heyd, G. E. Scuseria, and M. Ernzerhof, Hybrid functionals based on a screened Coulomb potential, J. Chem. Phys. **118**, 8207 (2003).
[39] A. Ubaldini and M. M. Carnasciali, Raman characterisation of powder of cubic RE_2O_3 (RE = Nd, Gd, Dy, Tm, and Lu), Sc_2O_3 and Y_2O_3, J. Alloys Compd. **454**, 374 (2008).
[40] P.-Y. Chen, T. Hadamek, S. Kwon, F. Al-Quaiti, A. B. Posadas, M. J. Kim, A. A. Demkov, and J. G. Ekerdt, Role of template layers for heteroepitaxial growth of lanthanum oxide on GaN (0001) via atomic layer deposition, J. Vac. Sci. Technol., A **38**, 012403 (2020).
[41] A. Walsh, J. L. F. Da Silva, S.-H. Wei, C. Körber, A. Klein, L. F. J. Piper, A. DeMasi, K. E. Smith, G. Panaccione, P. Torelli, D. J. Payne, A. Bourlange, and R. G. Egdell, Nature of the band gap of In_2O_3 revealed by first-principles calculations and X-ray spectroscopy, Phys. Rev. Lett. **100**, 167402 (2008).
[42] S. C. Dixon, A. Jiamprasertboon, C. J. Carmalt, and I. P. Parkin, Luminescence behaviour and deposition of Sc_2O_3 thin films from scandium(III) acetylacetonate at ambient pressure, Appl. Phys. Lett. **112**, 221902 (2018).
[43] V. H. Mudavakkat, V. V. Atuchin, V. N. Kruchinin, A. Kayani, and C. V. Ramana, Structure, morphology and optical properties of nanocrystalline yttrium oxide (Y_2O_3) thin films, Opt. Mater. **34**, 893 (2012).
[44] C. R. Michel and A. H. Martínez-Preciado, CO sensing properties of novel nanostructured La_2O_3 microspheres, Sens. Actuators, B **208**, 355 (2015).
[45] Scientific Group Thermodata Europe, *Thermodynamic Properties of Inorganic Materials* (Springer-Verlag, Berlin, Heidelberg, 1999), Vol. 19.
[46] J. Y. Zhu, F. Liu, and G. B. Stringfellow, Dual-surfactant effect to enhance p-type doping in III-V semiconductor thin films, Phys. Rev. Lett. **101**, 196103 (2008).
[47] J. Zhu, F. Liu, G. B. Stringfellow, and S.-H. Wei, Strain-enhanced doping in semiconductors: Effects of dopant size and charge state, Phys. Rev. Lett. **105**, 195503 (2010).
[48] O. Neufeld and M. C. Toroker, Play the heavy: An effective mass study for α-Fe_2O_3 and corundum oxides, J. Chem. Phys. **144**, 164704 (2016).
[49] Y. Kumar, M. Pal, M. Herrera, and X. Mathew, Effect of Eu ion incorporation on the emission behavior of Y_2O_3 nanophosphors: A detailed study of structural and optical properties, Opt. Mater. **60**, 159 (2016).